24th June 2015

Hydrodynamic Microgap Voltammetry under Couette Flow Conditions: Electrochemistry at a Rotating Drum in Viscous Poly-(Ethylene-Glycol)

Christopher E. Hotchen[a], H. Viet Nguyen[b], Adrian C. Fisher[b*], Paul E. Frith[a], and Frank Marken[a*]

[a] Department of Chemistry, University of Bath, Claverton Down, Bath BA2 7AY, UK
[b] Department of Chemical Engineering, University of Cambridge, New Museums Site, Pembroke Street, Cambridge, CB2 3RA, UK

To be submitted to ChemPhysChem
Proofs to F. Marken

F.Marken@bath.ac.uk

Abstract

Electrochemical processes in highly viscous media such as poly-(ethylene glycol) (here in PEG200) are interesting for energy conversion applications, but problematic due to slow diffusion causing low current densities. Here, a hydrodynamic microgap experiment based on Couette flow is introduced for an inlaid disc electrode approaching a rotating drum. Steady state voltammetric currents are independent of viscosity and readily increased by two orders of magnitude with further potential to go to higher rotation rates and nanogaps. Quantitative theory is derived for the prediction of currents under high shear Couette flow conditions and generalised for different electrode shapes. The 1,1'-ferrocene-dimethanol redox probe in PEG200 (D = 1.4 × 10^{-11} m^2 s^{-1}) is employed and data are compared with (i) a Levich-type equation expressing the diffusion-convection limited current and (ii) a COMSOL® simulation model providing a potential dependent current trace.

Keywords: poly-ethylene-glycol, green solvent, ferrocene, voltammetry, Couette, electrodeposition, poly-electrolyte.

Content Entry:

Graphical Abstract:

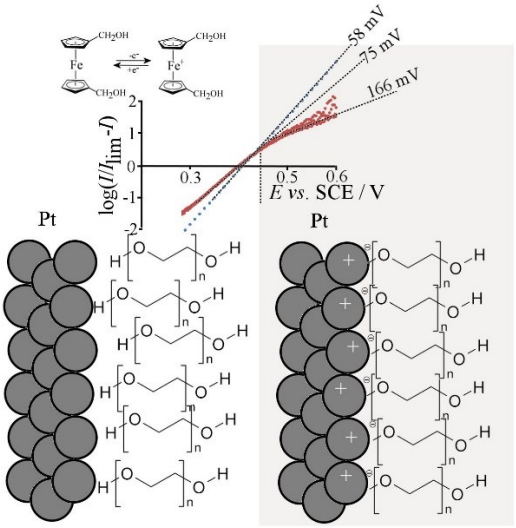

High shear conditions under Couette flow are employed for hydrodynamic voltammetry in poly-ethylene-glycol to reveal "stickiness" of solvent molecules on platinum at potential positive of 0.45 V vs. SCE.

1. Introduction

Electrochemical processes in poly-(ethylene glycol) (or PEG) media[1] have been reported in the literature in studies of viscosity effects,[2] non-Newtonian effects,[3] and in ionic melts.[4] "Protected" PEGs with alkylated terminal alcohol groups have been studied as electrolyte[5] and can be applied in energy storage technologies[6] or as gel electrolytes in solar cells.[7] Surface immobilised PEGs have been employed in sensors[8] and for controlling electrochemical surface reactivity.[9] PEGs generally may be considered very benign and low-cost, low-volatility industrial solvent media with many interesting properties including (i) ability to absorb moisture,[10] (ii) ability to bind carbon dioxide,[11,12] and (iii) introducing resistance of surfaces to biofouling.[13] In this report PEG200 (poly-(ethylene-glycol) with molecular weight 200 g mol^{-1}) is employed as a model viscous liquid to demonstrate the current enhancement in a hydrodynamic microgap under Couette flow conditions. The main aim of the work is to introduce a new quantitative tool for the exploration of high current density redox processes in highly viscous media. We also demonstrate novel effects associated with the use of "large" solvent molecules.

Hydrodynamic methods are important in electrochemistry for the quantitative study of electrode processes at rotating disc or rotating ring-disc systems,[14] at wall-jet[15] and wall-tube[16] experiments, in channel flow devices with one or more coupled electrodes under well-defined microfluidic conditions,[17,18,19] in sono-electrochemistry[20] and in microwave-enhanced electro-chemistry,[21] as well as in electroanalysis with vibrating electrodes.[22] We have recently proposed a rocking disk alternative to the rotating disk first for the uniform deposition of photocathode absorber layers[23] and for hydrodynamic modulation.[24] An important distinction can be made between (i)

electrode systems with approximately uniform diffusion layer thickness (e.g. the rotating disc electrode) and (ii) electrode systems with non-uniform diffusion layer thickness (for example in channel flow electrodes[25]). For static electrodes with a flow across the surface, a high current density is always observed at the leading edge with a diffusion layer that is increasing towards the trailing edge. Therefore the resulting current is dependent not only on the area, but also on the shape of the electrode. For each type of electrode a typical "Levich-type" equation can be derived to account for geometric and flow parameters.[26]

The problem with many conventional hydrodynamic voltammetry experiments in highly viscous media is that most of the known methods become unsuitable due to the *macroscopic* flow pattern being affected (i.e. with container wall effects becoming significant at high viscosity and macroscopic flow pattern changing). Therefore an approach based on a *microscopic* flow pattern (viscosity-independent) is realised here for "Couette flow" (that is laminar flow between two moving plates as seen for example in SECM[27]) in a microgap.

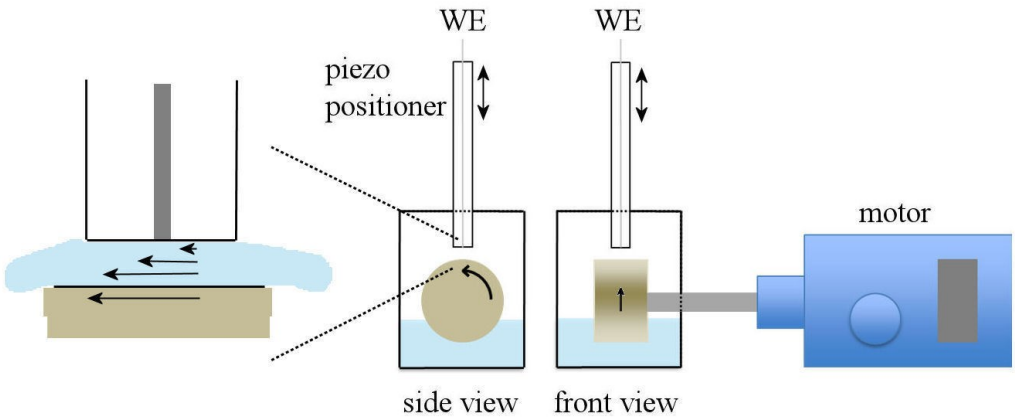

Figure 1. A schematic drawing of the rotating drum rig. The distance between the electrode and the drum is controlled by a piezoelectric positioner. The frequency of rotation can also be controllably varied.

A novel hydrodynamic microgap system based on a rotating drum (see Figure 1) is proposed where an inlaid disc electrode (250 μm diameter platinum sealed into glass) is positioned with a piezo translator to be at constant distance from a rotating drum. The drum takes viscous liquid from a reservoir and produces a high shear region (Couette flow region) at the point where the electrode is placed. Both the rotation speed and the electrode-drum microgap distance are important parameters in the hydrodynamic process and current enhancements of up to two orders of magnitude are observed when going to smaller gaps and higher rotation rates. A quantitative Levich-type expression for the diffusion-convection controlled limiting current is derived and a COMSOL® simulation for voltammetric responses is proposed and compared to experimental data.

2. Experimental

2.1. Reagents

1,1'-Ferrocene-dimethanol (Aldrich, 98%) was used as a reversible redox species in liquid poly(ethylene glycol) (Sigma-Aldrich, average molecular weight = 200 g mol^{-1}) with 20 mM lithium perchlorate (Sigma-Aldrich, ACS reagent, ≥ 95%) as background electrolyte. Potassium ferricyanide(III) ($K_3Fe(CN)_6$, Aldrich, 99+ %) was employed as redox species in aqueous solutions containing 1 M potassium nitrate (KNO_3, Sigma-

Aldrich, ≥ 99.0 %) as background electrolyte. Experiments were performed at 20 +/- 2 ^{o}C.

2.2. Instrumentation

All electrochemical measurements were recorded using an Autolab PGSTAT12 potentiostat. An Edwards vacuum pump ES50 was used to reduce the pressure in the vacuum voltammetry cell to ca. 0.8 mbar. For rotating drum experiments, a Physik Instrumente E-665 piezo-positioner (500 μm travel distance) was used to control the distance between the working electrode (250 μm diameter platinum disc) and the rotating drum to the nearest 0.1 μm. For voltammetry in ambient conditions a three-electrode set up was employed with a Pt wire counter electrode and a KCl-saturated calomel electrode (SCE) reference. The rotation of the drum was controlled by an IKA®-WERKE EUROSTAR digital overhead stirrer, which allowed the frequency of rotation to be adjusted to the nearest revolution per minute (rpm). Diffusion coefficient analysis was performed using the electrochemical simulation software DigiElch (version 4.9). COMSOL-Multiphysics® modelling software was used to simulate voltammetry under hydrodynamic conditions.

2.3. Procedure for Voltammetry in Vacuum

In order to measure reliable diffusion coefficient and concentration data in PEG media, an electrochemical cell was designed for voltammetry to be carried out *in vacuo* at room temperature for solutions with a low vapour pressure using a two-electrode arrangement (Figure 2). Voltammetric measurements were performed in a 40 μL droplet of solution placed onto the surface of the 100 μm diameter Pt disc working electrode (sealed in glass). The system was subjected to 3 h of vacuum prior to experimentation in order to

remove unwanted gases, such as oxygen, and control the humidity level of the system (to lower capacitive current background signals). The voltammetry *in vacuo* was otherwise unaffected but helped reduce background interference when determining the diffusion coefficient of 1,1'-ferrocene-dimethanol in PEG200 (Figure 2). Losses due to evaporation of either PEG200 solvent or 1,1'-ferrocene-dimethanol remained insignificant for over 12 h duration of experimentation *in vacuo*. A silver wire counter/pseudo-reference electrode was used for chronoamperometry and cyclic voltammetry currents < 10 nA. Figure 2B-D show that voltammograms obtained under ambient conditions and *in vacuo* are consistent (therefore no change in viscosity, which is ca. 48 cP at 25 ºC[28]) and DigiElch 4.0 analysis[29] of chronoamperometry data gives $D = 1.4 \times 10^{-11}$ m^2 s^{-1} for 1,1'-ferrocene-dimethanol under these conditions.

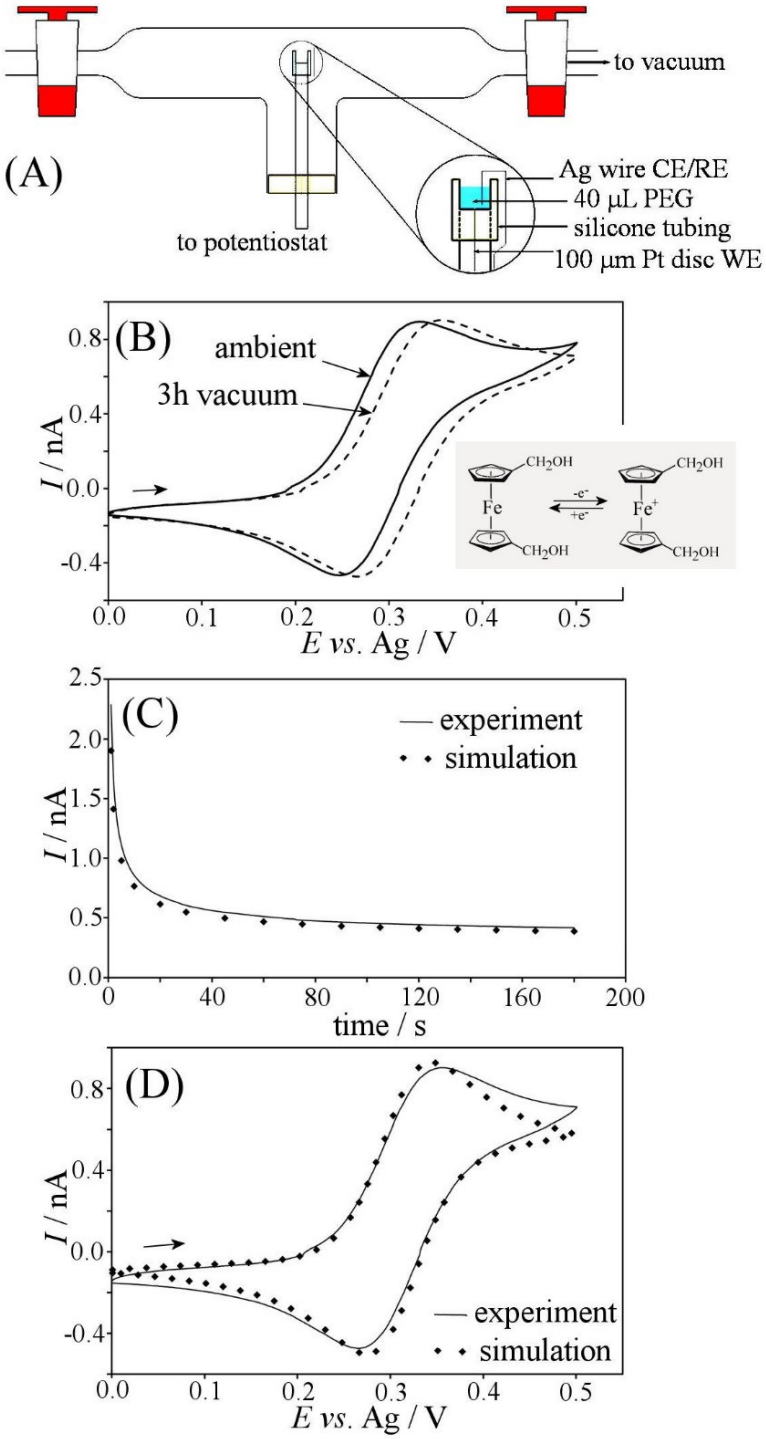

Figure 2. (A) Schematic diagram of the electrochemical cell used for voltammetry *in vacuo*. The solution was a 40 µL droplet of PEG200 on the surface of the working electrode. (B) Cyclic voltammograms (scan rate 10 mV s^{-1}) for oxidation of 1 mM 1,1'-ferrocene-dimethanol in PEG200 under ambient conditions and *in vacuo*. (C) Chronoamperometry data (potential step 0.0 to +0.5 V vs. Ag) with simulation fit. (D) Cyclic voltammograms for experimental (solid line) and simulated (♦) data for $D = 1.4 \times 10^{-11}$ m^2 s^{-1}.

2.4. Procedure for Hydrodynamic Microgap Voltammetry

Hydrodynamic microgap voltammetry was performed using the apparatus shown in Figure 1. The system consisted of a motor with a digital readout of the rotation speed, which could be adjusted to the nearest revolution per minute (rpm). The motor is connected via an axle to a 50 mm diameter solid polyether-ether-ketone (PEEK) wheel, which is partially submerged in the solution. This wheel rotates, collecting a thin film of solution on the surface of the wheel. The working electrode (250 μm diameter Pt) is positioned above the apex of the drum such that the active area of the electrode is at a tangent to the rotating wheel. The distance, *h*, between the electrode and wheel was controlled to the nearest 0.1 μm by a piezoelectric positioner with a maximum gap of 500 μm. Residual eccentricity in the drum rotational movement is estimated to be below 5 μm (which is below 10% of the smallest distance *h* employed in this study) and assumed insignificant at least in first approximation, as are effects from drum roughness and curvature. The working electrode was polished using alumina paste (0.3 μm diameter), rinsed and dried using nitrogen prior to experimentation. A saturated calomel reference electrode (SCE) and Pt counter electrode were positioned in the bulk solution. All electrochemical measurements were performed in an earthed Faraday cage to reduce background interferences. During the course of experimentation in PEG200 an increase in temperature with longer periods of drum rotation was noted (dissipation of energy into heat) and therefore a waiting time in between experiments was employed to keep the temperature of the solution within 20 ^{o}C to 25 ^{o}C. Additional temperature effects locally in the high shear region are possible, but are ignored here.

3. Theory

3.1. Derivation of a Levich-type Expression

Depending on the hydrodynamic conditions and the voltage scan rate, the collected current approaches a pseudo-steady state value I_{lim}. Two classical cases in the literature are those of the rotating disk electrode (RDE, equation 1)[30] and the rectangular flow channel electrode (equation 2).[31]

$$I_{lim,RDE} = 1.554nFAc_0D^{\frac{2}{3}}f^{\frac{1}{2}}v^{-\frac{1}{6}} \quad (1)$$

$$I_{lim,FCE} = 0.925nFAc_0D^{\frac{2}{3}}\left(\frac{4v_f}{h_c^2 d_c x_e}\right)^{\frac{1}{3}} \quad (2)$$

In these expressions the mass transport limited current (I_{lim}) is expressed in terms of the number of electrons transferred per molecule diffusing to the electrode surface (n), the Faraday constant (F), the electrode area (A), the bulk concentration of redox active species (c_{o}), the diffusion coefficient (D), the electrode width and length (w_{e} and x_{e}, respectively, inherent in A), the rotation frequency in Hz (f), the solution viscosity (v), the volume flow rate (v_f), and the channel height and channel width (h_c and d_c respectively). In order to obtain a similar expression for the hydrodynamic microgap under Couette flow conditions[27] simplified parameters need to be defined. The set-up for the rotating drum experiment is inherently three dimensional. However, one can simplify the model to two dimensions as follows. If the gap between the inlaid disc electrode and the drum is sufficiently smaller than both the electrode outer diameter and the diameter of the drum, then the curvature effect can be ignored. The key parameters employed here are the drum diameter (50 mm), the outer diameter of the electrode casing (4 mm), and the distance from electrode to rotating drum (50 to 500

μm). Under these conditions the Reynold number $Re = \frac{U_0 \times h}{v}$ (with drum speed U_0 = 2π drum radius × frequency ≈ 10 ms^{-1}, distance h, and kinematic viscosity v ≈ 0.05 Pa s) is less than 1000 thereby satisfying laminar flow requirements.

It is assumed that the flow within the microgap is adequately described by Couette flow (ignoring problems due to drum curvature and the development of the steady state flow profile with time). Under these conditions, the liquid is confined between two closed boundaries, one of which is moved at a constant velocity relative to the other. Couette flow is a shear-induced flow and the velocity profile under steady-state conditions is a simple linear function (Figure 3).

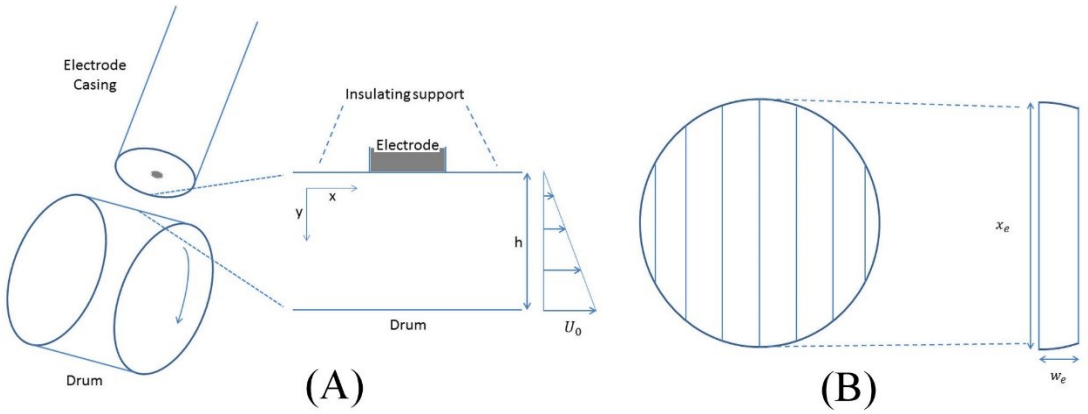

Figure 3. (A) Experimental set-up and 2D model simplification with the Couette flow field. (B) Dividing the inlaid disc electrode into rectangular electrodes of length x_e.

The derivation follows methods employed in previous studies.[32] To simplify the calculation, assume the electrode has a uniform width into the page (Figure 3B) and a rectangular geometry. Considering the mass transport under steady state condition and the coordinates in Figure 3, the transport equations are given in equation 3.

$$U\frac{\partial C_i}{\partial x} = D_i\frac{\partial^2 C_i}{\partial y^2} \quad (3)$$

Here $C_i = C_O, C_R$ denotes the concentration of oxidative and reductive species undergoing an electrochemical transformation (equation 4).

$$\mathrm{R} \rightleftharpoons \mathrm{O} + e^- \quad (4)$$

Taking into account the Couette flow conditions, the boundary conditions can be expressed as shown in equations 5 to 9.

$$U_0\frac{y}{h}\frac{\partial C_R}{\partial x} = D_R\frac{\partial^2 C_R}{\partial y^2} \quad (5)$$

$$U_0\frac{y}{h}\frac{\partial C_O}{\partial x} = D_O\frac{\partial^2 C_O}{\partial y^2} \quad (6)$$

$$y \to \infty\text{: } C_R \to C_0, C_O \to 0 \quad (7)$$

$$y = 0\text{: } D_R\frac{\partial C_R}{\partial y} + D_O\frac{\partial C_O}{\partial y} = 0 \quad (8)$$

$$y = 0\text{: } \frac{C_R}{C_0} = \exp\left(-\frac{nF}{RT}(E - E^0)\right) = \exp(-\theta) \quad (9)$$

Here θ denotes the dimensionless voltage, E^0 is the equilibrium voltage of redox couple (4) and E is the externally applied voltage. Equation (7) can be satisfied given that the gap h is a few times larger than the diffusion layer $\delta_{diff} = (\frac{Dhx_e}{U_0})^{\frac{1}{3}}$. The variable transformation (10) is introduced into equations (5) and (6) to give (11) and (12).

$$\eta = \left(\frac{U_0}{xh}\right)^{1/3} y \tag{10}$$

$$\frac{1}{3D_R}\eta^2 \frac{\partial C_R}{\partial \eta} + \frac{\partial^2 C_R}{\partial \eta^2} = 0 \tag{11}$$

$$\frac{1}{3D_O}\eta^2 \frac{\partial C_O}{\partial \eta} + \frac{\partial^2 C_O}{\partial \eta^2} = 0 \tag{12}$$

Solving (11) and (12) subject to boundary conditions (7) yields equations (13) and (14).

$$\frac{C_R - C_R(\mathrm{y}=0)}{C_0 - C_R(\mathrm{y}=0)} = \frac{\int_0^{\eta} \exp\left(-\frac{\eta^3}{9D_R}\right) d\eta}{\int_0^{\infty} \exp\left(-\frac{\eta^3}{9D_R}\right) d\eta} \tag{13}$$

$$\frac{C_O - C_O(\mathrm{y}=0)}{-C_O(\mathrm{y}=0)} = \frac{\int_0^{\eta} \exp\left(-\frac{\eta^3}{9D_O}\right) d\eta}{\int_0^{\infty} \exp\left(-\frac{\eta^3}{9D_O}\right) d\eta} \tag{14}$$

Using an additional variable transformation (15) with $D_i = D_O, D_R$ the definite integral then becomes the Gamma function (16).

$$s = \frac{\eta^3}{9D_i} \tag{15}$$

$$\int_0^{\infty} \exp\left(-\frac{\eta^3}{9D_i}\right) d\eta = \left(\frac{D_i}{3}\right)^{1/3} \int_0^{\infty} s^{-2/3}\exp(-s)\, ds = \left(\frac{D_i}{3}\right)^{1/3} \frac{\Gamma\left(\frac{1}{3}\right)}{\left(\frac{1}{9}\right)^{\frac{1}{3}}} \tag{16}$$

By expanding the integrals in the numerator into polynomial series and integrating term by term, one can finally obtain the concentration distribution for R and O, respectively. The flux at the electrode surface is thus calculated as in equations (17) and (18).

$$D_R \frac{\partial C_R}{\partial y}(y=0) = 0.5384 D_R^{\frac{2}{3}} \left(\frac{U_0}{xh}\right)^{\frac{1}{3}} \left(C_0 - C_R(\mathrm{y}=0)\right) \tag{17}$$

$$D_O \frac{\partial C_O}{\partial y}(y=0) = 0.5384 D_O^{\frac{2}{3}} \left(\frac{U_0}{xh}\right)^{\frac{1}{3}} \left(-C_O(\mathrm{y}=0)\right) \tag{18}$$

Combining (17) and (18) with (8) and (9) to solve for C_R, C_O, then substituting back the values into one of the expressions above, the flux at the electrode is obtained as equation (19).

$$D_R \frac{\partial C_R}{\partial y}(y=0) = 0.5384 D_R^{\frac{2}{3}} \left(\frac{U_0}{xh}\right)^{\frac{1}{3}} C_0 \frac{\exp(\theta)}{\exp(\theta) + (\frac{D_R}{D_O})^{2/3}} \tag{19}$$

Finally, integrating the above expression across the electrode surface gives the current at a given potential as equation (20).

$$\begin{aligned} I &= nFw \int_0^{w_e} D_R \frac{\partial C_R}{\partial y}(y=0)dx \\ &= 0.8076 nFw D_R^{\frac{2}{3}} U_0^{\frac{1}{3}} x_e^{\frac{2}{3}} h^{-\frac{1}{3}} C_0 \frac{\exp(\theta)}{\exp(\theta) + (\frac{D_R}{D_O})^{\frac{2}{3}}} \end{aligned} \tag{20}$$

At very highly oxidizing potentials (i.e. large $\exp(\theta)$) the transport limiting current simplifies to equation (21) with area $A = w_e \times x_e$ and velocity $U_0 = 2\pi R$ where R = 25 mm is the rotating drum diameter.

$$I_{lim,rectangle} = 0.8076nFC_0AD_R^{\frac{2}{3}}\left(\frac{U_0}{hx_e}\right)^{\frac{1}{3}} \quad (21)$$

This equation for rectangular electrodes is very closely related to equation 2 for the channel flow case and it offers a general access to various other shapes of electrodes by combination of thin rectangular strips. For example, numerical summation over individual parts of the disk (see Figure 3B) using equation 21 immediately gives the corresponding Levich-type equation 22 for the inlaid disc electrode (with r_0 the radius) in the hydrodynamic microgap under Couette flow conditions.

$$I_{lim,disk} = 0.6866nFC_0AD_R^{\frac{2}{3}}\left(\frac{U_0}{hr_0}\right)^{\frac{1}{3}} \quad (22)$$

Furthermore, comparison of equation 21 and equation 22 allows the "magic rectangle" case with current density equal to that of a disk of equal area to be determined as a w_e/x_e = 1.1863. That is, a simulation of a rectangle with *electrode width* = 1.1863 × *electrode length* will automatically give steady state current responses identical to that for a circular disk electrode of the same area. This simplification will be used for COMSOL® simulations.

3.2. COMSOL® Simulation

COMSOL® is a multi-physics modelling software and is applied here to verify the expression (21) for the rectangular electrode. The simplified 2D model in Figure 3 is coded in COMSOL® with open boundary conditions at open ends. At the moving boundary, constant sliding velocity U_0 is applied. Similarly, zero velocity condition is used for the stationary electrode casing. Meshing of the simulation domain is based on the finite element approach (FE) to solve partial differential equations (PDEs). Couette flow is simple and the usual unstructured triangular mesh is sufficient. Fine meshing is applied at the boundaries and a structured mesh is used to resolve the fluid boundary layers (see Figure 4A,B).

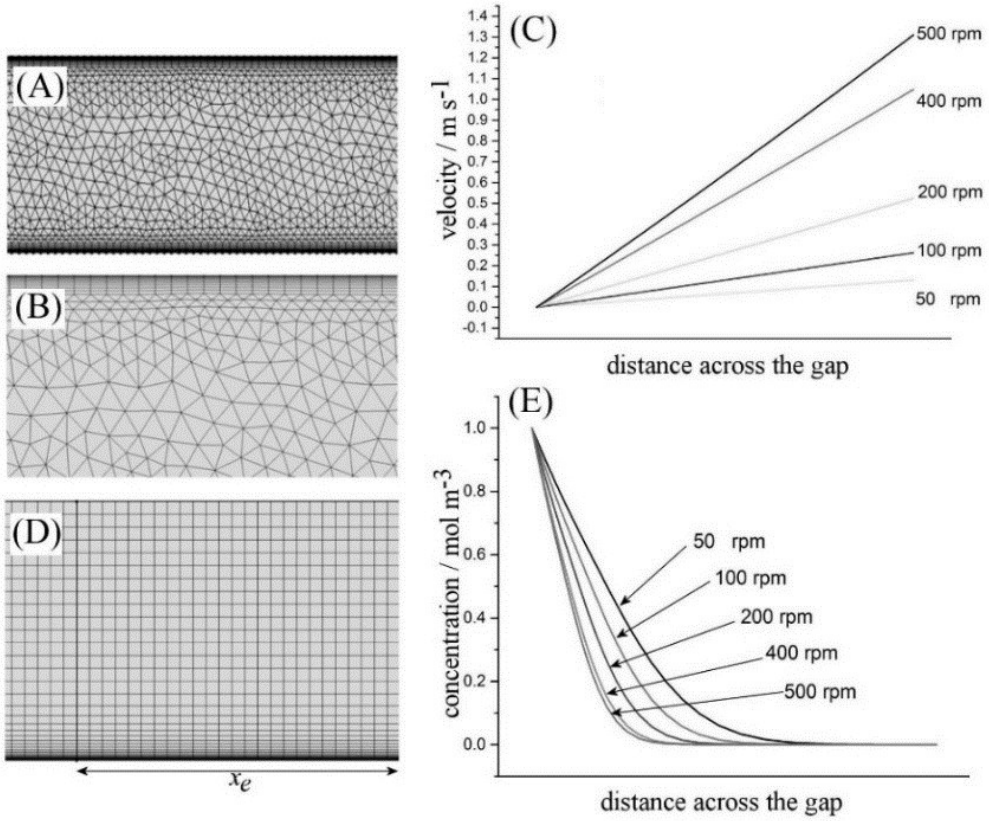

Figure 4. Triangular mesh used for COMSOL® computation of Couette Flow. Overall mesh structure (A) and enlargement of the top and bottom edges (B). (C) Velocity profiles at $h = 500$ μm and at various drum rotating rates. (D) Structured mesh used for mass transport calculations. Nodes are denser above electrode surface (bottom) and sparser towards the moving bulk (top). (E) Concentration profile for the oxidised form of 1,1'-ferrocene-dimethanol at the trailing edge for h = 500 μm and various drum rotation rates.

Figure 4 shows that the velocity profiles for a given *h* and different rotating frequencies have indeed linear behaviour with respect to the dimension across the gap. The computation makes use of the Electrochemistry Module in COMSOL®, which is specifically developed for electrochemical analysis and related problems. Electrochemical phenomena can be described by the general Nernst-Planck-Poisson (NPP) equation (equation 23).

$$\frac{\partial C_i}{\partial t} = \nabla.(D_i \nabla C_i) - \underline{v}.\nabla C_i + \frac{zF}{RT}\nabla.(D_i C_i \nabla E) \qquad (23)$$

If sufficient salt is added to the solution, the migration flux (i.e. the third term) can be ignored, leaving only the familiar diffusion (1st) and convective (2nd) terms. Due to the fluid dynamics having a much shorter time scale compared to mass transport, the Couette flow field $\underline{v}$ can be solved separately and then used as input to solve equation (23). A generic quadrilateral mesh is generated and used for all the mass transport computation. To completely resolve the diffusion layer, a sufficiently small element size near the electrode surface is required. One can estimate such dimension using expression based on $\delta_{diff} = (\frac{D \times h \times x_e}{U_0})^{1/3} \approx (\frac{10^{-11} \times 10^{-4} \times 10^{-4}}{10})^{1/3} \approx 10^{-7} m$ and thus the smallest element size should be in the order of 10^{-7} m. Thus the mesh for our mass transport computation is structured as follows. Normal to the electrode surface, an exponential mesh with smallest element size of 10^{-7} m is employed. Furthermore, the element-size growth rate is set to be 1.2, so as to allow for adequate resolution of the diffusion layer. In the direction across the surface, a regular spacing is used. The spacing is chosen such that at least 250 points cover the electrode surface and thus

ensure accurate convergence of the current values. The electrochemistry at the electrode is described by the classical Butler-Volmer equation. Oxidation of 1,1'-ferrocene-dimethanol is expected to have a symmetrical transition state, hence the charge transfer constant is set to be $\alpha = 0.5$ in the Butler-Volmer model with the heterogeneous standard rate constant set to 1 ms^{-1} assuming the limiting case of reversible conditions. The Levich expression 22 is then verified using different combinations of gap h and drum rotation rates ω (see Table 1 below). The results show a good agreement (within 2%) between the numerical and theoretical values for the limiting current. The key to accuracy in this simulation is in the meshing for the electrochemical process (Figure 4D) and the fact that a high current density is expected at the leading edge of the electrode. Coarse meshing can lead to an underestimation of the total current.

Table 1. Comparison between the COMSOL® simulated limiting current and the Levich-type equation 21.

Gap h / μm	Rotation rate ω / rpm	Rotation rate / s^{-1}	$I_{Simulated}/I_{Levich}$
50	50	0.833	1.019
50	500	83.3	0.999
500	50	0.833	1.020
500	500	83.3	1.002

To verify the extent of the diffusion layer thickness across the microgap system between electrode and rotating drum under the conditions employed here, the concentration of the oxidised form of 1,1'-ferrocene-dimethanol versus position across the gap (at the trailing edge) has been plotted for different rotation rates (Figure 4E).

4. Results and Discussion

4.1. Hydrodynamic Microgap Voltammetry I.: $Fe(CN)_6^{3-/4-}$ in Aqueous Electrolyte

In order to verify the theory based on Couette flow, the hydrodynamic microgap systems was tested with 5 mM ferricyanide ($K_3Fe(CN)_6$) as the redox species in an aqueous solution with 1 M KNO_3 as electrolyte (equation 24)

$$Fe(CN)_6^{3-} + e^- \rightleftharpoons Fe(CN)_6^{4-} \quad (24)$$

The distance, *h*, between the 250 μm diameter Pt disc working electrode and the rotating drum was initially fixed at 50 μm, whilst the rotation frequency was varied. Cyclic voltammetry measurements were taken using rotation frequencies between 50 and 400 revolutions per minute (rpm). In Figure 5A it is shown that limiting currents increased by more than one order of magnitude compared to those recorded in a static solution. Figure 5B shows that the limiting reduction current is proportional to the cube root of the rotation frequency of the rotating drum consistent with equation 22. The dotted line shows the theoretical values for a diffusion coefficient of $D = 0.65 \times 10^{-9}$ m^2s^{-1}.[33]

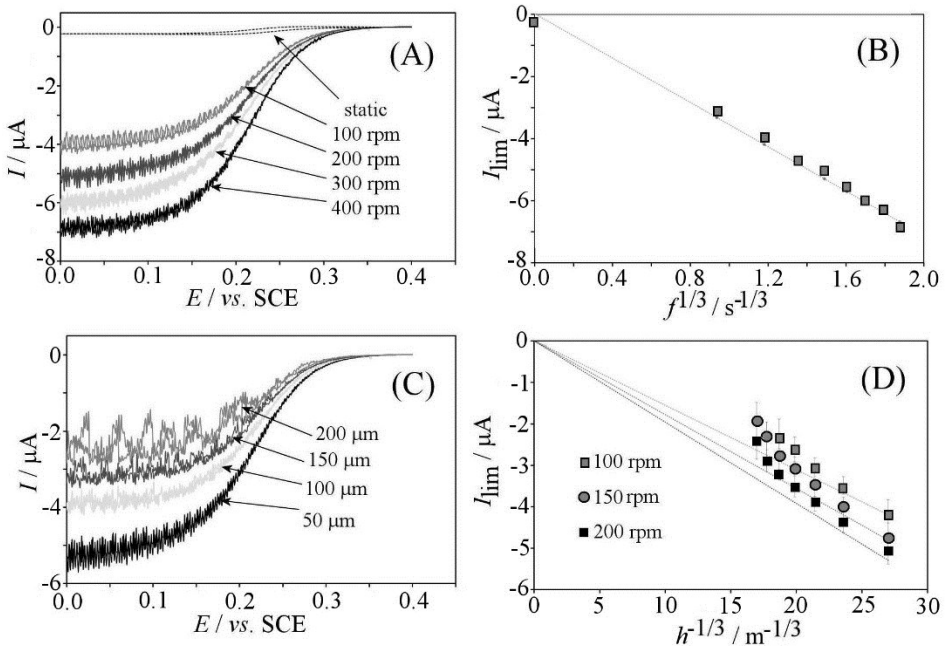

Figure 5. (A) Cyclic voltammograms (scan rate 10 mVs^{-1}; 250 µm diameter platinum disk; 50 µm microgap) for reduction of 5 mM $K_3Fe(CN)_6$ in 1 M KNO_3 in static solution (dotted) and with a rotation frequency of (i) 100, (ii), 200, (iii) 300 and (iv) 400 rpm. (B) Plot of the limiting current (at 0.0 V vs. SCE) for experimental results versus cube root of the rotation frequency in Hz with a dotted line indicating calculated limiting currents based on equation 22 (with $D = 0.65 \times 10^{-9}$ m^2s^{-1}). (C) Cyclic voltammograms (scan rate 10 mVs^{-1}; 50 rpm) for reduction of 5 mM $K_3Fe(CN)_6$ in 1 M KNO_3 with (i) 50, (ii) 100, (iii) 150 and (iv) 200 µm. (D) Plot of the limiting current (at 0.0 V vs. SCE) at 100 rpm, 150 rpm, and 200 rpm versus reciprocal cube root of the distance with dotted lines indicating calculated limiting currents based on equation 22.

Next, the effect of the microgap was investigated. Figure 5C shows voltammograms for the reduction of 5 mM $Fe(CN)_6^{3-}$ with increasing microgap becoming more "noisy" which is indicative for a loss of laminar conditions at wider gap distances for the aqueous solution of relatively low viscosity. The plot in Figure 5D confirms some deviation at wider hydrodynamic gap for all three rotation rates. Additional problems due to not fully established laminar Couette flow for wider microgaps are possible. However, overall, the agreement between theory and experiment is good and measurements in more viscous PEG200 are possible.

4.2. Hydrodynamic Microgap Voltammetry II.: 1,1'-Ferrocene-dimethanol in PEG Electrolyte

Having determined the diffusion coefficient for 1,1'-ferrocene-dimethanol in PEG200, the same system was investigated under hydrodynamic conditions using the hydrodynamic gap experiment with a 250 µm diameter Pt disk electrode and a gap of 500 µm. The rotation frequency of the drum was varied between 50 rpm and 500 rpm. Cyclic voltammograms for the oxidation of 1 mM 1,1'-ferrocene-dimethanol under hydrodynamic conditions show steady state characteristics (Figure 6A) and a limiting current typically 50 times larger than those observed under static conditions. A comparison to the COMSOL simulation and to the limiting current predicted by equation 22 shows good agreement. There is some evidence for some irreversibility in the electron transfer, but the possible reason for this is discussed in more detail below.

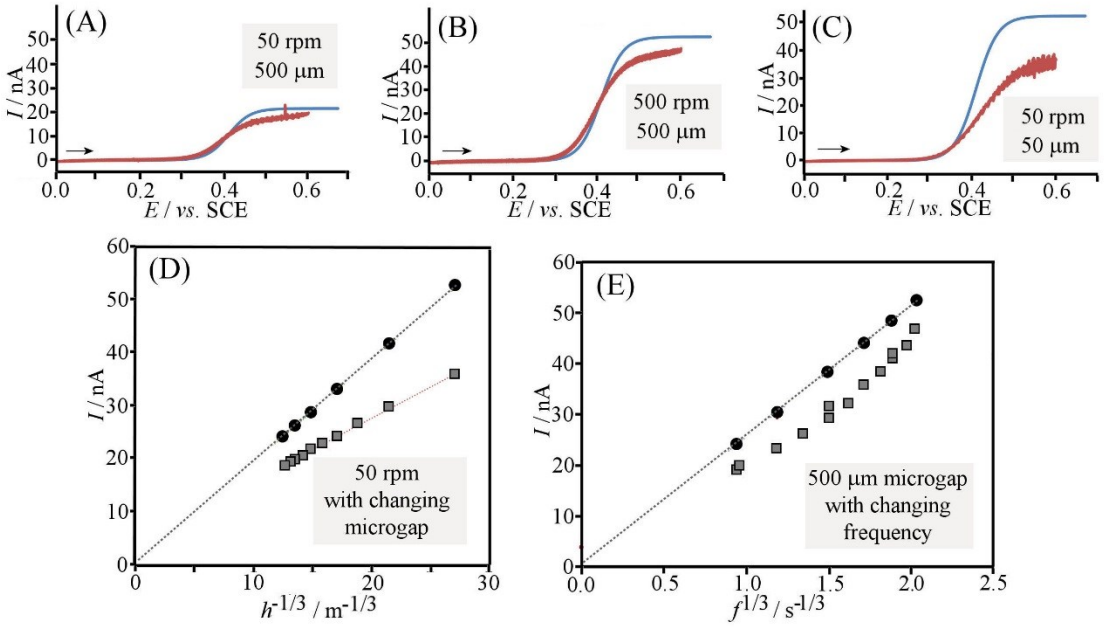

Figure 6. Cyclic voltammograms (scan rate 10 mVs^{-1}; comparison of experiment and COMSOL simulation) for oxidation of 1 mM 1,1'-ferrocene-dimethanol in PEG200 with 20 mM $LiClO_4$ at a 250 µm diameter platinum disk electrode under rotating drum conditions: (A) 500 µm gap, 50 rpm, (B) 500 µm gap, 500 rpm, (C) 50 µm gap, 50 rpm. (D) Plot of limiting currents (experimental at 0.6 V vs. SCE and theory) versus $h^{(-1/3)}$ at 50 rpm. (E) Plot of limiting currents (experimental at 0.6 V vs. SCE and theory) versus $f^{(-1/3)}$ at 500 µm gap.

A plot of the limiting current as a function of the inverse cube root of microgap distance (Figure 6D) shows that a mismatch of theoretical limiting current and experimental limiting current is observed going to small gaps (higher shear conditions). Data in Figure 6B and 6C also show that the apparent irreversibility in the electron transfer to 1,1'-ferrocene-dimethanol is more obvious for smaller gaps and for higher rotation frequency. When plotting the frequency dependency (Figure 6E) a relatively good agreement is seen, although all data points are below those predicted by theory. Given the accurate determination of the diffusion coefficient, this is unlikely to be the cause for the deviation. Problems with local energy dissipation or not-fully developed laminar flow are possible but cannot explain all of the results. In order to further explain the deviation between experiment and theory for the oxidation of 1,1'-ferrocene-dimethanol in PEG200 a log-plot analysis is shown in Figure 7 for data in Figure 6B. The simulation data clearly shows the anticipated 58 mV (= $RT/nF \times 2.303$) slope consistent with fully reversible electron transfer. However, the log-plot for 1,1'-ferrocene-dimethanol is split into two regions. Below 0.45 V vs. SCE a slope value of 75 mV is indicative of a transition to irreversible electron transfer. Above 0.45 V vs. SCE the slope changes to 166 mV, which cannot be reconciled with slow electron transfer. Instead it is likely that here the underlying interaction of the platinum surface with the PEG200 solvent changes (see schematic drawing) causing an additional impedance and therefore a deviation from the expected theoretical limiting current. A similar transition in mechanism is present in all experimental data sets and therefore likely to be associated with the partitioning of the 1,1'-ferrrocene-dimethanol molecule into the surface PEG200 layer. The considerable (average) size of the PEG200

molecules immobilised at the electrode surface is responsible for this "big solvent effect" being observed not only as slower electron transfer but also as an apparent lowering in the mass transport. This effect is most pronounced under high mass transport conditions (= short time scale) either for a small microgap or for high rotation rates. Note that the mass transport conditions under hydrodynamic gap conditions employed here correspond to a diffusional time scale of approximately 1 ms which is why data in chronoamperometry (Figure 2C) are less affected.

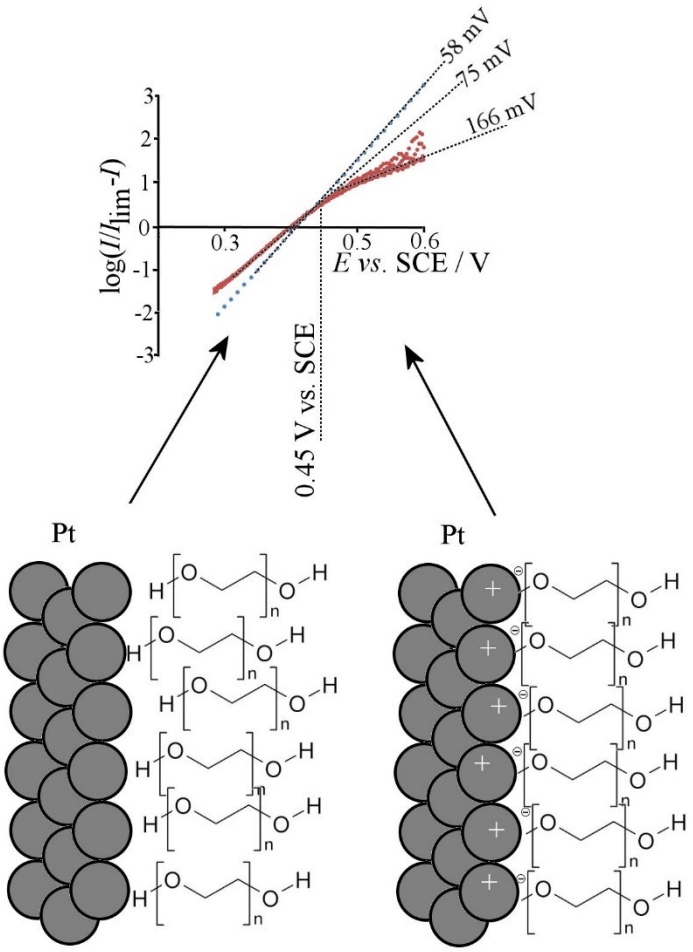

Figure 7. Log plot data for data in Figure 6B indicating a switch in mechanism at 0.45 V vs. SCE. Also shown are schematic drawings of the proposed chemical changes at the platinum PEG200 interface.

4. Conclusion

It has been shown that high mass transport limited currents can be achieved in highly viscous PEG media with the help of a hydrodynamic microgap system. A novel viscosity-independent approach based on a rotating drum and a piezo-controlled electrode position system has been developed. A quantitative model has been proposed based on Couette flow and realised (i) in terms of a Levich-type equation and (ii) as COMSOL® simulation. Both theory approaches are fully consistent and verified with a $Fe(CN)_6^{3-/4-}$ redox system in aqueous electrolyte.

When studying the redox chemistry of 1,1'-ferrocene-dimethanol in viscous PEG200 considerable current enhancements were noticed. A reliable diffusion coefficient was determined under static conditions, which was then employed under hydrodynamic conditions. Although the trends in experiment and in theory are generally in agreement, there is a marked deviation at potentials higher than 0.45 V vs. SCE and this has been attributed to a change in the conditions at the platinum – PEG200 electrolyte interface.

Further work will be required (i) to further verify the Couette flow system quantitatively for a wider range of solvents and redox systems, and (ii) to explore the new type of interface for a wider range of applications for PEG solvents. The system will also be of interest for application in other types of polymer solvents and for viscous ionic liquids. The development of a hydrodynamic "nano-gap" system would be very interesting, but this will require improved precision in the rotation mechanism.

Acknowledgements

C.E.H gratefully acknowledges the University of Bath for funding this research. H.V.N thanks Trinity College, Cambridge for funding his PhD study.

References

[1] J.M. Harris (ed.), *Poly(ethylene glycol) Chemistry: Biotechnical and Biomedical Applications*. Plenum Press, New York, 1992.

[2] K. Aoki, Y. Guo, J.Y. Chen, *J. Electroanal. Chem.* **2009**, *629*, 73.

[3] Y. Guo, K. Aoki, J.Y. Chen, T. Nishiumi, *Electrochim. Acta*, **2011**, *56*, 3727.

[4] W. Wang, D. Lee, R.W. Murray, *J. Phys. Chem. B*, **2006**, *110*, 10258.

[5] P. Los, G. Zabinska, A. Kisza, L. Christie, A. Mount, P.G. Bruce, *Phys. Chem. Chem. Phys*. **2000**, *2*, 5449.

[6] Y. Kato, S. Yokoyama, H. Ikuta, Y. Uchimoto, M. Wakihara, *Electrochem. Commun*. **2001**, *3*, 128.

[7] Y.T. Shi, C. Zhan, L.D. Wang, B.B. Ma, R. Gao, Y.F. Zhu, Y. Qiu, *Phys. Chem. Chem. Phys.* **2009**, *11*, 4230.

[8] M. Okazaki, K. Maruyama, M. Tsuchida, N. Tsubokawa, *Polymer J.* **1999**, *31*, 672.

[9] C.E. Hotchen, I.J. Maybury, G.W. Nelson, J.S. Foord, P. Holdway, F. Marken, *Phys. Chem. Chem. Phys.* **2015**, *17*, 11260.

[10] L. Ninni, H. Burd, W.H. Fung, A.J.A. Meirelles, *J. Chem. Eng. Data,* **2003**, *48*, 324.

[11] O. Aschenbrenner, P. Styring, *Energy Environm. Sci.* **2010**, *3*, 1106.

[12] Z.Z. Yang Q.W. Song, *Capture and Utilization of Carbon Dioxide with Polyethylene Glycol*, Springer Verlag, Berlin 2012.

[13] S. Krishnan, C.J. Weinman, C.K. Ober, *J. Mater. Chem.* **2008**, *18*, 3405.

[14] N.V. Rees, R.G. Compton, *Russ. J. Electrochem.* **2008**, *44*, 368.

[15] J.C. Ball, R.G. Compton, C.M.A. Brett, *J. Phys. Chem.* **1998**, *102*, 162.

[16] J.V. Macpherson, N. Simjee, P.R. Unwin, *Electrochim. Acta* **2001**, *47*, 29.

[17] J.A. Cooper, R.G. Compton, *Electroanalysis*, **1998**, *10*, 141.

[18] C. Amatore, N. Da Mota, C. Lemmer, C. Pebay, C. Sella, L. Thouin, *Anal. Chem.* **2008**, *80*, 9483.

[19] C. Amatore, N. Da Mota, C. Sella, L. Thouin, *Anal. Chem.* **2007**, *79*, 8502.

[20] R.G. Compton, J.C. Eklund, F. Marken, *Electroanalysis* **1997**, *9*, 509.

[21] I.J. Cutress, F. Marken, R.G. Compton, *Electroanalysis* **2009**, *21*, 113.

[22] D.E. Williams, K. Ellis, A. Colville, S.J. Dennison, G. Laguillo, J. Larsen, *J. Electroanal. Chem*. **1997**, *432*, 159.

[23] C.Y. Cummings, G. Zoppi, I. Forbes, D. Colombara, L.M. Peter, F. Marken, *Electrochim. Acta* **2012**, *79*, 141.

[24] S.D. Ahn, P.E. Frith, A.C. Fisher, A.M. Bond, F. Marken, *J. Electroanal. Chem.* **2014**, *722*, 78.

[25] I. Streeter, R.G. Compton, *Phys. Chem. Chem. Phys.* **2007**, *9*, 862.

[26] C.M.A. Brett, A.M.O. Brett, *Electrochemistry: Principles, Methods, and Applications*. Oxford University Press, Oxford, 1993.

[27] C. Combellas, M. Fermigier, A. Fuchs, F. Kanoufi, *Anal. Chem*. **2005**, *77*, 7966.

[28] S. Ottani, D. Vitalini, F. Comelli, C. Castellari, *J. Chem. Eng. Data,* **2002**, *47*, 1197.

[29] J. Weber, A.J. Wain, F. Marken, *Electroanalysis,* **2015**, DOI: 10.1002/elan.201500190.

[30] V.G. Levich, *Physiochemical Hydrodynamics*, Prentice Hall, Inc., Englewood Cliffs, N.J. 1962.

[31] R.G. Compton, E. Laborda, K.R. Ward, *Understanding Voltammetry: Simulation of Electrode Processes*, Imperial College Press, 2014.

[32] W.J. Blaedel, L.N. Klatt, *Anal. Chem*. **1966**, *38*, 879.

[33] R.N. Adams, *Electrochemistry at Solid Electrodes*, Marcel Dekker, New York, 1969, p. 220.